spectral characteristics in this case were the same as for the first configuration.

There is considerable scope for further improvement of the performance of this filter. First, the excess loss of the FPS can be reduced to a level of <0.2dB through improved fabrication techniques. Secondly, there are a number of advantages to writing the Bragg gratings directly into the coupler arms. This would automatically avoid the splice losses currently incurred, and by writing both gratings simultaneously it can be ensured that they are identical and that the arm lengths are equal, minimising polarisation mode dispersion. A compact, low loss and environmentally stable transmission filter can be fabricated in which the polarisation rotation and balancing of the two arms may be simply achieved by twisting the fibre. In addition, this device allows the relaxation of the interferometric matching requirements that are present in the Michelson interferometer-based filter mentioned earlier.

In conclusion we have demonstrated a low loss bandpass transmission filter based on a fibre polarisation splitter and fibre Bragg gratings. The total loss of our prototype device was ~1.2dB and we believe that with careful design this could be reduced below 0.5dB.

Acknowledgments: This work was supported by the EPSRC. The couplers were constructed using an IRE-POLUS Fusion Coupler Workstation. We would like to thank A. Kusnetsov for assistance with installation.

5 July 1994

Electronics Letters Online No: 19941017

M. J. Guy, S. V. Chernikov and J. R. Taylor (*Femtosecond Optics Group, Imperial College, London SW7 2BZ, United Kingdom*)

R. Kashyap (*British Telecom Laboratories, Martlesham Heath, Ipswich IP5 7RE, United Kingdom*)

References

1 HILL, K.O., FUJII, Y., JOHNSON, D.C., and KAWASAKI, B.S.: 'Photosensitivity in optical fibre waveguides: application to reflection filter fabrication', *Appl. Phys. Lett.*, 1978, **32**, pp. 647–648

2 KASHYAP, R., ARMITAGE, J.R., CAMPBELL, R.J., WILLIAMS, D.L., MAXWELL, G.D., AINSLIE, B.J., and MILLAR, C.A.: 'Light-sensitive optical fibres and planar waveguides', *BT Technol. J.*, 1993, **11**, (2), pp. 150–160

3 HILL, K.O., MALO, B., BILODEAU, F., and JOHNSON, D.C.: 'Photosensitivity in optical fibres', *Ann. Rev. Mater. Sci.*, 1993, pp. 125–157

4 MOREY, W.W., BALL, G.A., and MELTZ, G.: 'Photoinduced Bragg gratings in optical fibres', *Optics & Photonics News*, 1994, **5**, (2), pp. 8–14

5 OUELLETTE, F.: 'Dispersion cancellation using linearly chirped Bragg grating filters in optical waveguides', *Opt. Lett.*, 1987, **12**, pp. 847–849

6 EGGLETON, B., KRUG, P.A., and POLADIN, L.: 'Dispersion compensation by using Bragg-grating filters with self-induced chirp'. Tech. Dig. Opt. Fibre Commun. Conf., 1994, p. 227

7 KASHYAP, R., CHERNIKOV, S.V., MCKEE, P.F., and TAYLOR, J.R.: '30 ps chromatic dispersion compensation of 400fs pulses at 100Gbit/s in optical fibres using an all fibre photo-induced chirped reflection grating', *Electron. Lett.*, 1994, **30**, (13), pp. 1078–1080

8 BILODEAU, F., HILL, K.O., MALO, B., JOHNSON, D.C., and ALBERT, J.: 'High-return-loss narrowband all-fibre bandpass Bragg transmission filter', *IEEE Photonics Technol. Lett.*, 1994, **6**, pp. 80–82

9 ARCHAMBAULT, J.-L., RUSSELL, P. ST. J., HUA, P., and REEKIE, L.: 'Grating-frustrated coupler: a novel channel-dropping filter in single-mode optical fibre', *Opt. Lett.*, 1994, **19**, pp. 180–182

10 BRICHENO, T., and BAKER, V.: 'All-fibre polarisation splitter/combiner', *Electron. Lett.*, 1985, **21**, pp. 251–252

11 YATAKI, M.S., PAYNE, D.N., and VARNHAM, M.P.: 'All-fibre polarising beamsplitter', *Electron. Lett.*, 1985, **21**, pp. 249–251

Novel approach for increased dynamic range in optoelectronic sensing applications

A. Bonen, R.E. Saad, K.C. Smith and B. Benhabib

Indexing terms: Optical sensors, Automatic gain control

A novel approach is proposed to significantly increase the dynamic range of optoelectronic sensors. The power of the light source is monitored in a dynamic intensity-control loop designed to perform 'floating-point' measurements according to the attenuation in the optical path. The sensor acquires the combined dynamic ranges of the detector and light-source circuits.

Introduction: Presently, optoelectronic transducers seem to be the most appropriate for a wide range of sensing tasks. In particular, optoelectronic transducers that measure the light attenuation in an optical path are commonly used by robotic sensors [1–4]. The performance of optical transducers, however, is limited by the electronic interface to the computer-control algorithm. Electronic interfaces presently available are generally imperfect in ways which limit the realisation of the sensors' goals.

From an interface viewpoint, the transducer is a communication channel which connects a transmitter to a receiver. However, unlike in other cases of optical communication, data generation in optoelectronic sensors occurs inside the channel and not in the transmitter. Moreover, the data itself are analogue in nature. These facts impose special demands on the receiver circuits; nonlinearities commonly used by digital-communication circuits (such as for increasing the dynamic range through automatic-gain control) are strictly forbidden in the analogue channel.

While dynamic range (DR) is a very important parameter for any sensor, it is particularly critical for sensors measuring optical attenuation. The light intensity at the receiving end of such sensors is a strong function of many parameters. For example, it is inversely related to the square of the distance between the transducer's transmitter and its receiver [3]. Thus, even a modest distance operating range of 10:1 would result in a 100:1 range of light intensity at the receiver. This 20 dB optical power variation corresponds to a 40dB electrical measurement range. Other parameters, such as overall reflectivity and surface orientation, can cause the received light intensity to vary in an even more extreme manner. In fact, so extreme are the variations that it can be easily concluded that no fully-linear receiver circuit can possibly supply the required DR. Therefore, the DR of such sensors has, until now, been restricted by the DR of the receiver in the electronic interface.

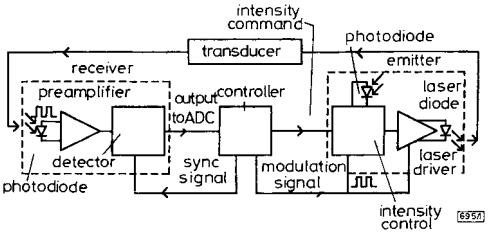

Fig. 1 *Block diagram*

Proposed design: Our design of a modulated transducer interface (Fig. 1) incorporates a new method: namely 'dynamic transmitter-intensity control' by which we eliminate the dependency in the receiver's DR and allow substantial widening of the sensor's DR. Unlike in conventional optical communication, the transmitter and the receiver for a sensory application are both subject to the same controller. The light-source intensity can be adjusted in real time; such that the light intensity at the receiver is adequate for measurement. This method results in an overall DR that is the sum of the DRs of the receiver and transmitter circuits.

A smart design can take advantage of the extended DR now available in the transmitter. Common receiver-design tradeoffs, such as balancing DR against high sensitivity and linearity, can be replaced by maximisation of other parameters at the expense of

the DR. However, the DR extension occurs in the transmitter only, and therefore we restrict our further discussion to an analysis of the transmitter circuit.

A few pseudo-arbitrary decisions had to be made for the construction of the prototype circuit presented in this Letter. For example, we chose 830nm as the operating optical wavelength, because a vast selection of optoelectronic components is available for this wavelength. Likewise, the proposed transmitter-circuit design is based on the use of a laser diode (LD). However, if desired, the driver circuit can be adapted to drive a light-emitting diode (LED) instead. The above, and the following choices of electrical components, are in no way unique, nor do they restrict the applicability of the design to any specific sensor.

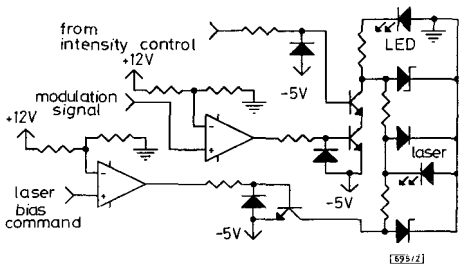

Fig. 2 *Laser-driver circuit*

Laser driver: Fig. 2 shows the laser-driver circuit. The LD used is the Hitachi HL8312G. It is capable of emitting 20mW of optical power. The current driving the LD is composed of a constant biasing current and a modulated intensity current. The biasing current is driven through a transistor switch, and is set such that it induces just above minimal lasing from the LD. This minimises turn-on effects, and reduces temperature variations in the LD. The signal from the intensity-control circuit is modulated by another transistor switch. Two Zener diodes protect the LD from overdrive. The commands to control the two switching transistors are converted from TTL levels and supplied by the control circuit.

It is critical that the power supply connected to the receiver circuit is not affected by the high-current LD signal. Any such effect can cause the modulated signal to be picked up by the sensitive low-noise receiver circuit. Therefore, the −5V power source that supplies the LD current should be used in the transmitter circuit only.

Intensity control: The transmitter circuit, shown in Fig. 3, operates as a closed loop for light-intensity control. A photodiode, integrated with the LD, provides feedback for the control by capturing a small portion of the generated light. A transimpedance amplifier biases the photodiode and converts its sample into a voltage signal. The gain of this amplifier is adjusted to allow the largest voltage span that will not saturate the later stages.

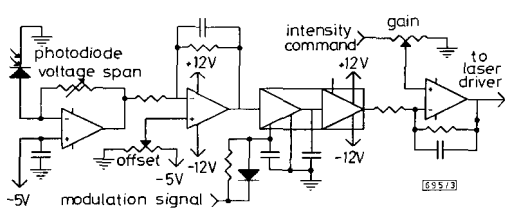

Fig. 3 *Intensity-control circuit*

A lowpass filter is used in the next stage to attenuate any high-frequency noise picked up by the transimpedance amplifier. This stage also incorporates an offset adjustment to set the zero level of the output intensity. Accurate adjustment of this zero level is essential for obtaining the maximum possible DR in the transmitter.

The control loop is periodically broken in the laser-driver stage by the modulation. To prevent this on-off switching from affecting the intensity control, we added a sample-and-hold circuit (S&H) ahead of the intensity comparator. About 3μs after the LD is turned on, the S&H becomes transparent to the feedback signal. This delay is needed to allow both the LD and the input stages to stabilise. When the LD is turned off, the S&H is switched to the hold state, and retains the 'on' feedback value until the next modulation cycle.

The comparator stage is the heart of the intensity-control circuit. Here, the feedback signal is continuously compared to the desired intensity, and any disagreement causes an adjustment in the signal relayed to the laser driver. The pole frequency of the lowpass filter sets the time constant by which new intensity command comes into effect, and therefore should not be too low. However, this frequency has to be under the modulation frequency, such that the comparator behaves as an integrator and smoothes out any intensity variations related to the light modulation. The maximum intensity command is matched here to the maximum current allowed by the laser driver by gain adjustment.

Circuit performance: The performance of the proposed circuit design was analysed by investigating the frequency response, noise, DR, and time-domain performance. The intensity command was taken from the output of a 12 bit D/A converter, and a square wave was used for modulation. Because the noise from the transmitter circuit proved to be negligible at any output intensity, the full 12 bit range was used in the intensity control.

The frequency response of the transmitter is limited mainly by the delay and slew rate of the operational amplifiers and by the delay of the S&H chip. Although the operation of the laser driver was still possible at frequencies up to 500kHz, the intensity control lost most of its linearity above 200kHz. Thus, the use of a faster S&H chip and faster opamps with a higher slew rate is recommended for modulation frequencies above 10kHz. The 4096:1 range of light power emitted by the transmitter works to increase the DR of the sensor by 72dB (electrical measurement). An even greater improvement in the DR is possible by using a higher precision D/A converter and S&H chip.

Application example: The proposed electronic interface circuit was built and interfaced to an experimental robotic proximity sensor [4]. This sensor uses measured optical attenuation (in the paths from a single transmitter to eight receivers) to calculate the distance and orientation of a surface in relation to the sensor's transducer.

Measurements were acquired at various points within a range corresponding to 1–100mm distance and ±30° orientation (a set of five measurements at each point). A 10min warm-up period was allowed before taking measurements. Control of the LD output power was aimed at obtaining maximum SNR in the measurements. Therefore, for each set of measurements the LD output power was adjusted such that the received signals were as strong as possible without any of them being saturated. The measurements were repeated three times at roughly 24h intervals.

The measurements were digitised by a 12 bit A/D converter, analysed, and yielded the following results: The noise level in each set of measurements was ±1 LSB. Thus, the SNR was 66dB for the strong signals and as low as 32dB for weak signals. Measurements taken on different days had ±2 LSB variation, reducing the above SNRs by 6dB. The added 1 bit noise was presumably a result of drifts and temperature variations in the interface circuits.

Conclusions: A novel transmitter for a sensor interface was designed as a practical low-cost circuit for use by a variety of optoelectronic sensors. As shown by experimentation, the development and implementation of the proposed unique technique can double the dynamic range usually achieved by a conventional sensor interface.

29 June 1994

Electronics Letters Online No: 19940996

A. Bonen, R.E. Saad, K.C. Smith and B. Benhabib (*Computer Integrated Manufacturing Laboratory, Department of Mechanical Engineering, University of Toronto, 5 King's College Road, Toronto, Ontario M5S 1A4, Canada*)

References

1 HIROSE, S., and YONEDA, K.: 'Development of optical 6-axial force sensor and its signal calibration considering non-linear interference'. IEEE Int. Conf. Robotics and Automation, Cincinnati, USA, May 1990, pp. 46–53

2 RUSSELL, R.A.: 'Robot tactile sensing' (Prentice-Hall, Australia, 1990)

3 PARTAATMADJA, O., BENHABIB, B., SUN, A., and GOLDENBERG, A.A.: 'An electro-optic orientation sensor for robotics', *IEEE Trans. Robotics and Automation*, 1992, **8**, (1), pp. 111–119

4 BONEN, A., SMITH, K.C., and BENHABIB, B.: 'Development of a robust electro-optical proximity sensor'. IEEE Int. Conf. Intelligent Robots and Systems, Yokohama, Japan, July 1993, pp. 986–990

High alignment tolerance coupling scheme for multichannel laser diode/singlemode fibre modules using a tapered waveguide array

J.-M. Cheong, J.-W. Seo and Y.-K. Jhee

Indexing terms: Optical couplers, Packaging

A high alignment tolerance scheme for coupling a laser diode array to a singlemode fibre array using a tapered waveguide array as an intermediate coupling device is proposed. The numerical results show a 0.5dB lateral alignment tolerance of ±6μm and maximum coupling efficiency of –8.6dB.

Introduction: The most difficult problem in realising laser-fibre array modules for optical parallel interconnections is how to realise an efficient and high alignment tolerance optical technique for coupling a laser diode (LD) array to a singlemode fibre (SMF) array. An attractive approach to passive alignment to obtain low cost and compact packaging is provided by the flipchip solder-bump technique [1]. In this technique, the vertical positional accuracy required for laser alignment to fibre, which depends on control of the thickness of the deposited solder, can be achieved with the aid of standoffs provided on the substrate [2]. However, accurate lateral selfalignment without relatively precise initial positioning is very difficult because the small surface area of the laser chip does not permit a large number of large-diameter solder bumps which guarantee repreducible precision. From these points of view, a high alignment tolerance scheme for coupling the LD array to the SMF array needs to be investigated. For this purpose, a coupling scheme has been realised whereby a tapered waveguide array is placed between the LD array and the fibre array is proposed in this Letter. Combining the beam propagation method (BPM) and the effective-index method, the coupling characteristics of the LD into the waveguide are anaysed.

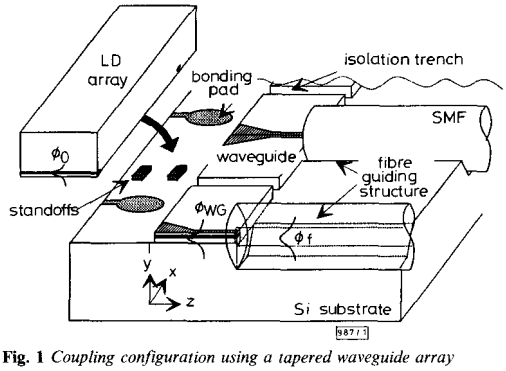

Fig. 1 *Coupling configuration using a tapered waveguide array*

LD/SMF array packaging scheme: A schematic diagram of the structure for coupling the LD array to the SMF array on a silicon substrate is illustrated in Fig. 1. A tapered waveguide array is used as an intermediate coupling device located between the LD array and the SML array. To reduce the optical crosstalk between adjacent channels, the waveguides can be isolated from one another by trenches. Because the guiding structure on the terraced silicon substrate can be fabricated for the low-loss coupling of optical power from the waveguide to the SMF [3], silica-based waveguides on a silicon substrate are considered to be candidates for the proposed packaging scheme. The tapered waveguide geometry analysed is illustrated in Fig. 2. We take n_i as the effective refractive index of the tapered waveguide, and α as the ratio of the effective refractive index of the negative-index waveguides to n_i.

The principle of operation and the philosophy behind the high alignment tolerance in the coupling from the LD to the waveguide can be explained as follows. The negative-index waveguides designated by numbers 1 and 2 in Fig. 2 suppress the excitation of the higher-order modes in the tapered region for a highly misaligned input field, and the central negative-index waveguide 1 reduces the coupling efficiency to obtain a larger alignment tolerance for very small misalignments.

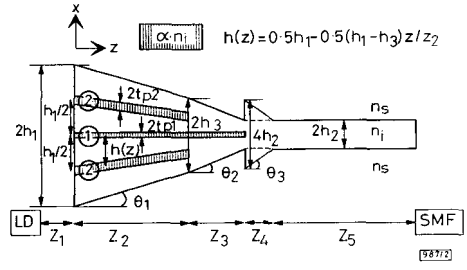

Fig. 2 *Tapered waveguide structure*

By controlling the anisotropic etching carefully [4], we can fabricate the guiding structures for fibres having a low coupling loss in the packaging process. Therefore, the packaging tolerance is mainly dependent on the alignment tolerance between the LD and the tapered waveguide.

Numerical results: Referring to Fig. 1, the total coupling efficiency η between the LD and the SMF is calculated as follows:

$$\eta = \eta_1 \cdot \eta_2 \tag{1}$$

where η_1 is the coupling efficiency of the LD into the waveguide and η_2 is the waveguide-to-fibre coupling efficiency. η_1 can be obtained from the overlap integral

$$\eta_1 = \frac{\left|\int_{-\infty}^{\infty} E^*(x)\cdot\phi_{WG}^{\parallel}(x)dx\right|^2}{\int_{-\infty}^{\infty}|\phi_o^{\parallel}(x)|^2dx\cdot\int_{-\infty}^{\infty}|\phi_{WG}^{\parallel}(x)|^2dx} \times \frac{\left|\int_{-\infty}^{\infty}\phi_o^{\perp *}(y)\cdot\phi_{WG}^{\perp}(y)dy\right|^2}{\int_{-\infty}^{\infty}|\phi_o^{\perp}(y)|^2dy\cdot\int_{-\infty}^{\infty}|\phi_{WG}^{\perp}(y)|^2dy} \tag{2}$$

where * denotes complex conjugation, $E(x)$ is the propagation field profile calculated by BPM, and $\phi_o^{\perp\parallel}$ and $\phi_{WG}^{\perp\parallel}$ are the fundamental eigenmode field profiles of the LD and the output waveguide, respectively. A coupling efficiency η_2 higher than 98% can be obtained using the modefield conversion technique [5], and this value is used in the calculation.

Because the divergent beam from the LD contains large-angle components for which the Fresnel approximation implied in the BPM is not valid [6], the results of our analysis will yield approximate values of the propagating electric-field distributions. In the numerical calculations, we use h_1 =8μm, h_2 = 1.5μm, h_3 = 3μm, t_{p1} = 0.5μm , t_{p2} = 1μm, z_2 = 200μm, z_3 = 150μm, z_4 = 170μm, n_s = 1.5, n_i = 1.51, α = 0.9955, θ_1 = 1.43°, θ_2 = 0.57°, θ_3 = 0.5° and the free-space wavelength λ_o = 1.3μm. Assuming Gaussian profiles for the LD power distributions in the directions parallel and perpendicular to the junction plane, the beam spot sizes ($\omega_o^{\parallel}$, $\omega_o^{\perp}$) corresponding to each direction are assumed to be 2 and 0.5μm, respectively. The modefield diameter of the SMF is assumed to be 9.8μm. Using the dispersive curves of step-index slab waveguide, the calculated thickness of the output waveguide satisfying the single-mode condition is ~3.8μm.